Engineering GaS crystal anisotropy via ultrafast laser excitation

KRISHNA P. KHAKUREL,[1,7] RAPHAEL CLADY,[2] SHIRLY ESPINOZA,[1] UDDHAB CHAULAGAIN,[1] AMELIE FERRE,[2] JAKOB ANDREASSON,[1] MARIA LUSORDO,[3] DILSON JUAN,[4,5] OLIVIER UTEZA,[2] AND YAEL GUTIERREZ[3,6,8]

[1]*ELI Beamlines Facility, The Extreme Light Infrastructure, ERIC, Za Radnicí 835, Dolní Břežany 25241, Czech Republic*
[2]*Aix-Marseille Université, CNRS, LP3, UMR7341, 13009 Marseille, France*
[3]*Istituto di Chimica della Materia Condensata e delle Tecnologie perl'Energia ICMATECNR, C. so Stati Uniti 4, Padova 35127, Italy*
[4]*Departamento de Física de la Materia condensada, Gerencia de Investigación y Aplicaciones, Centro Atómico Constituyentes, CNEA, Av. General Paz 1499, (1650) Villa Maipú, Provincia de Buenos Aires, Argentina*
[5]*Instituto de Nanociencia y Nanotecnología, Centro Atómico Constituyentes, CNEA-CONICET, Av. General Paz 1499, (1650) Villa Maipú, Provincia de Buenos Aires, Argentina*
[6]*Departamento de Física Aplicada, Universidad de Cantabria, Avenida de los Castros, s/n, Santander 39005, Spain*
[7]*krishna.khakurel@eli-beams.eu*
[8]*gvelay@unican.es*

Abstract: Gallium sulphide (GaS) is an emerging monochalcogenide material that has recently attracted interest in optical technologies due to its tunable bandgap in the near-UV region. In this work, we employ *in situ*, *in-operando* X-ray diffraction to investigate local atomic modifications in GaS induced by 400-nm femtosecond laser pulses. We identify the energy threshold at which irreversible structural changes occur and observe a laser-induced elongation of the unit cell along the *c*-axis. This elongation is expected to enhance the anisotropy of the material's physical properties. *Ab initio* calculations further reveal that the experimentally observed $\approx 10\%$ elongation along the *c*-axis leads to a transition from a direct to an indirect bandgap, accompanied by a bandgap increase of approximately 0.45 eV. Additional *ab-initio* optical simulations show that this structural transformation results in a nearly constant in-plane refractive index contrast of $\Delta n \approx 0.1$ across a wide spectral range, from the visible to the near-infrared, with negligible optical losses, which could be of interest for reconfigurable photonics applications.

1. Introduction

Crystalline-to-crystalline transformations in two-dimensional (2D) materials are emerging as a promising pathway for next-generation reconfigurable photonic and optoelectronic technologies, as they are expected to be faster and more energy-efficient than conventional amorphous-to-crystalline switching processes [1]. Among these materials, van der Waals (vdW) semiconductors such as the gallium monochalcogenides (i.e., gallium sulfide (GaS), gallium selenide (GaSe), and gallium telluride (GaTe)) are particularly appealing due to their broad and tunable bandgaps, high carrier mobilities, and strong light–matter interactions [2]. In particular, GaS has attracted increasing attention owing to its wide bandgap tunability from the visible to the near-UV range [3,4], intrinsic polymorphism [5], and excellent ambient stability [2].

These properties have already enabled GaS to be integrated into a variety of optoelectronic applications, including UV photodetectors with fast response times [6–10], nonlinear optical

devices [11], heterogeneous catalysts [12,13], and ultrafast mode-locked lasers operating at 1.55 µm [14]. More recently, GaS has been proposed as a wide bandgap phase-change material (PCM) capable of enabling reconfigurable on-chip photonic functionalities through light-induced amorphous-to-crystalline switching [15]. However, the potential to induce crystalline-to-crystalline transitions in GaS using ultrafast optical excitation remains largely unexplored. Demonstrating and understanding such transformations could represent a crucial step toward realizing low-energy, high-speed, and durable PCM-based platforms for reconfigurable photonics [1].

To unlock this potential, it is essential to gain insight into how light modifies GaS at the atomic level, particularly through reversible or irreversible structural reconfigurations. While recent efforts have investigated its nonlinear optical response and ultrafast carrier dynamics [16], direct experimental evidence of laser-induced structural transformations is still lacking.

In this work, we address this gap by combining *in-situ*, *in-operando* X-ray diffraction with *ab initio* calculations to investigate the structural and optical effects of femtosecond laser excitation in GaS. We identify the energy threshold required to trigger irreversible atomic rearrangements and observe a laser-induced elongation of the unit cell along the *c*-axis. First-principles calculations reveal that this $\approx 10\%$ elongation drives a transition from a direct to an indirect bandgap, accompanied by a bandgap increase of approximately 0.45 eV. Furthermore, optical simulations show that the resulting structural transformation yields an in-plane refractive index contrast of $\Delta n \approx 0.1$, nearly constant across the visible to near-infrared spectral range, with no optical losses. These findings highlight the potential of GaS as a reconfigurable photonic material driven by ultrafast crystalline-to-crystalline transitions.

2. Methods

2.1. Experimental set up

The experiments are performed at the ASUR platform of LP3 laboratory. The schematic of the experimental set-up is shown in Fig. 1.
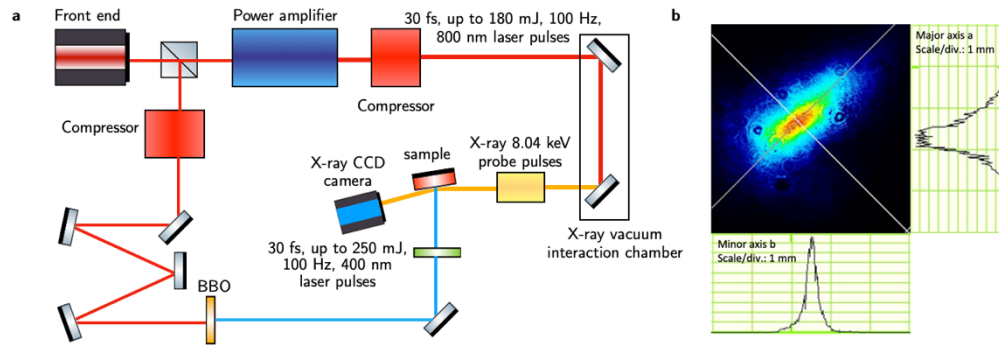

Fig. 1. (a) Schematic of the experimental setup. (b) The spatial 2D-distribution of the 400-nm fs pump laser in the sample plane (focused with a 100-cm UV lens), demonstrating an elliptical spot with a Gaussian-like distribution along the two transverse directions and free of any hot spots. Only the energy is varied to change the fluence on the sample during the experiment.

A 100-Hz, 30-fs, ≈ 180-mJ Ti:sapphire laser system is focused on a copper (Cu) disk to generate Cu-K$_\alpha$ radiation at the wavelength of 1.54 Å (8.04 keV). Benefiting from the fully synchronized multi-beamline capability of the ASUR platform [17], a second laser beam is used for preparing the pump beam. The 30-fs, 1-mJ pump beam is propagated through a 200-µm thick BBO crystal to generate the 400-nm, fs illumination used for the experiments. The choice of this wavelength

for the pump beam is to target above band-gap excitation of the GaS [5]. An optical focusing arrangement using a UV fused silica lens with a long focal length generates a large irradiation spot making it straight-forward to overlap the optical pump and X-ray probe beams at the surface of the sample. Neutral density filters are used to control the pump fluence driving the material transformation. The pump fluence is given by $F = E/\pi ab$, where E is the energy of the laser (measured before the experiment), and a and b, are the major and minor radius of the elliptical laser spot on the sample (measured with a charged coupled device (CCD) camera before each experiment). The sample is positioned on a 6-axis stage to control translational and rotational movements. A CCD X-ray detector (CEGITEK REBIRX 270 S 500 2D Hybrid Pixel Photon Counting Detector), equipped with a large chip size ($\approx 56\,\text{cm}^2$ with $130\,\mu\text{m} \times 130\,\mu\text{m}$ pixel size) is positioned about 10 cm from the sample center. To further enhance the signal-to-noise ratio, part of the divergent K_α X-ray probe is redirected by a one-dimensional (1D) multilayer X-ray Bragg optics (AXO-Dresden Gmbh, Germany) along a converging cone of $0.73°$ to a secondary focus of $\approx 75\,\mu\text{m}$ at the sample plane. This arrangement enables *in-situ* and *in-operando* measurement of the rocking curve of any peak of the diffracting (rotating) sample within a reasonable exposure time (10000 shots – 100 seconds).

2.2. Computational methods

Density functional theory (DFT) first principles calculations based on norm-conserving pseudopotentials (NCPP) [18] were carried out using the Quantum Espresso (QE) code [19]. Electronic exchange and correlation interaction was included at semi-local level with the generalized gradient approximation (GGA), using the exchange functional of Cooper (C09x) [20]. To account for dispersion interactions, we employ truly non-local correlations as given by Lee et al. (vdW-DF2) [21]. Core electrons are described by *ab-initio* optimized Vanderbilt pseudopotentials, generated following the recipe given by Hamann [22] in the Kleinman–Bylander fully non-local separable representation [23], available in the PSEUDODOJO online database [24] (version 0.4.1 of the ONCVPSP code). NCPP for Ga and S used in the calculations that involve vdW non-local dispersion interactions were generated with the ONCVPSP code [available on the website http://www.mat-simresearch.com/]. For Ga element, $3d^{10}\,4s^2\,4p^1$ are considered as valence electrons. Lighter chalcogenide S atom is constructed with an electronic configuration that includes six valence electrons ($3s^2\,3p^4$). Rhombohedral ($R\bar{3}m$) conventional standard ($\alpha = \beta = 90°$, $\gamma = 120°$) supercell of GaS with 12 atoms in total were employed through all the calculations. Brillouin zone integrations were carried out using a Monkhorst-Pack [25] Γ centered sampling of $14 \times 14 \times 2$ points and an energy cutoff for plane waves expansion of 90 Ry to attain converged results. Geometric parameters reported, namely interatomic distances and angles, were obtained by structural optimization, where atoms are allowed to relax until the maximum component of the force acting on any atom is smaller than 0.01 eV/Å. The frequency dependent dielectric tensor is obtained using perturbation theory with adiabatic turning on, as implemented in the post processing code *epsilon.x* [19]. In the limit of small non-vanishing excited states lifetime (Γ), the imaginary part of the dielectric tensor assumes the Drude-Lorenz form, if metal Drude-like intraband contributions are neglected:

$$\epsilon_{2\alpha,\beta}(\omega) = \frac{8\pi e^2}{\Omega N_{\mathbf{k}} m^2} \sum_{n \neq n'} \sum_{\mathbf{k}} \frac{\hat{\mathbf{M}}_{\alpha,\beta}}{(E_{\mathbf{k},n'} - E_{\mathbf{k},n})} \times \frac{\Gamma \omega f(E_{\mathbf{k},n})}{\left[(\omega_{\mathbf{k},n'} - \omega_{\mathbf{k},n})^2 - \omega^2\right]^2 + \Gamma^2 \omega^2} \quad (1)$$

and the real part can be calculated through a Kramers-Kronig transformation:

$$\epsilon_{1\alpha,\beta}(\omega) = 1 + \frac{2}{\pi} \int_0^\infty \frac{\omega' \epsilon_{2\alpha,\beta}(\omega')}{\omega'^2 - \omega^2} d\omega' \quad (2)$$

where Ω is the volume of the lattice cell, e the electric charge, m the electron mass, ω the laser frequency, $N_{\mathbf{k}}$ the number of k-points with frequency ω_k, while n and n' label valence and

conduction bands, respectively. The subscripts α and β indicate the different cartesian directions. $E_{\mathbf{k},n}$ are the Kohn-Sham eigenvalues of the DFT calculation, $f(E_{\mathbf{k},n})$ is the Fermi distribution function accounting for the occupation of the levels and the squared dipole matrix elements are defined, considering the periodic part of the single particle Bloch functions $|u_{\mathbf{k},n}\rangle$, as follows:

$$\hat{\mathbf{M}}_{\alpha,\beta} = \langle u_{\mathbf{k},n'}|\hat{\mathbf{p}}_{\alpha}|u_{\mathbf{k},n}\rangle\langle u_{\mathbf{k},n}|\hat{\mathbf{p}}_{\beta}^{\dagger}|u_{\mathbf{k},n'}\rangle \tag{3}$$

This formulation only accounts for **k**-momentum conserved independent interband transitions, neglecting local-field effects and electron-hole interaction (excitonic contribution) in the optical response.

3. Results

This study focuses on crystalline GaS thin films of thickness ≈ 500 nm and with rhombohedral symmetry (space group $R\bar{3}m$, N0166) grown with preferred c-axis orientation on a Si(100) substrate by chemical vapor deposition [5]. The unit cell of the $R\bar{3}m$ GaS is shown in Fig. 2(a). The crystalline structure of this semiconducting material is composed of covalently bonded S-Ga-Ga-S tetralayers, stacked along the c-axis and held together by weak van der Waals interactions.
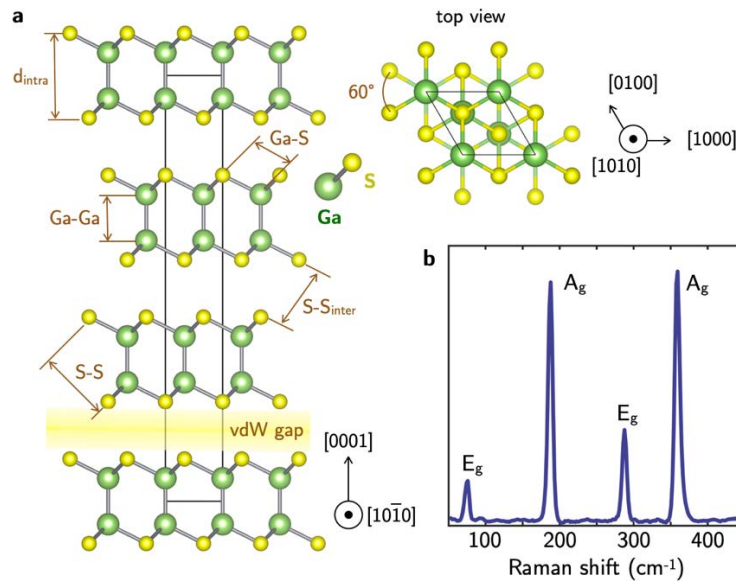

Fig. 2. (a) Side and top view of the unit cell of the rhombohedral $R\bar{3}m$ phase of GaS. Arrows indicate the bond distances reported in Table 1. (b) Raman spectra of the sample used for the experiment.

Within each tetralayer, the Ga atoms are aligned vertically on top of one another, while the sulfur atoms in the bottom layer are rotated by 60° relative to those in the top layer, as shown in the top-view projection. Consistently, the Raman spectrum of the studied films in Fig. 2(b) shows four Raman modes appearing at 76 (E_g), 188 (A_g), 289 (E_g) and 360 cm^{-1} (A_g), characteristic of the $R\bar{3}m$ GaS phase structure [5]. The tabulated unit cell lattice parameters for this phase are $a = b = 3.605$ Å and $c = 23.45$ Å [26], in good agreement with those measured in the films used in this study [5].

As later shown in Figs. 3 and 4, we measured the (003) diffraction peak of the GaS samples. The use of a large-area CCD X-ray detector enabled simultaneous acquisition of both transmitted

Table 1. Comparison of cell parameters (*a* and *c*), interatomic distances and angles between S-Ga-S and S-Ga-Ga obtained experimentally and by DFT in the case of $R\bar{3}m$ GaS without and with illumination. Distances are in Å, and angles in sexagesimal degrees labeled by the three defining atoms. The experimental and DFT distances and angles for the w/o illumination case are taken from Ref. [5].

	a	*c*	Ga-Ga	Ga-S	S-S	d_{intra}	S - S$_{inter}$	S-Ga-S	S-Ga-Ga
Exp. with illumination	-	25.380	-	-	-	-	-	-	-
DFT with illumination	3.594	25.380	2.442	2.346	5.074	4.630	4.356	100.01	117.80
Exp. w/o illumination	3.594	23.174	2.507	2.325	5.050	4.604	3.748	101.25	116.82
DFT w/o illumination	3.594	23.174	2.432	2.343	5.053	4.607	3.745	100.18	117.66

and diffracted X-ray signals, allowing for precise calibration of the diffraction peak position. The center of the rocking curve corresponding to the (003) reflection in the pristine material, obtained by averaging multiple measurements, was found at $\theta \approx 5.73°$. This angular position corresponds to a *c*-axis interplanar spacing of 23.174 Å, as calculated using Bragg's law and the rhombohedral plane-spacing formula [27], and in agreement with the value reported in [5].
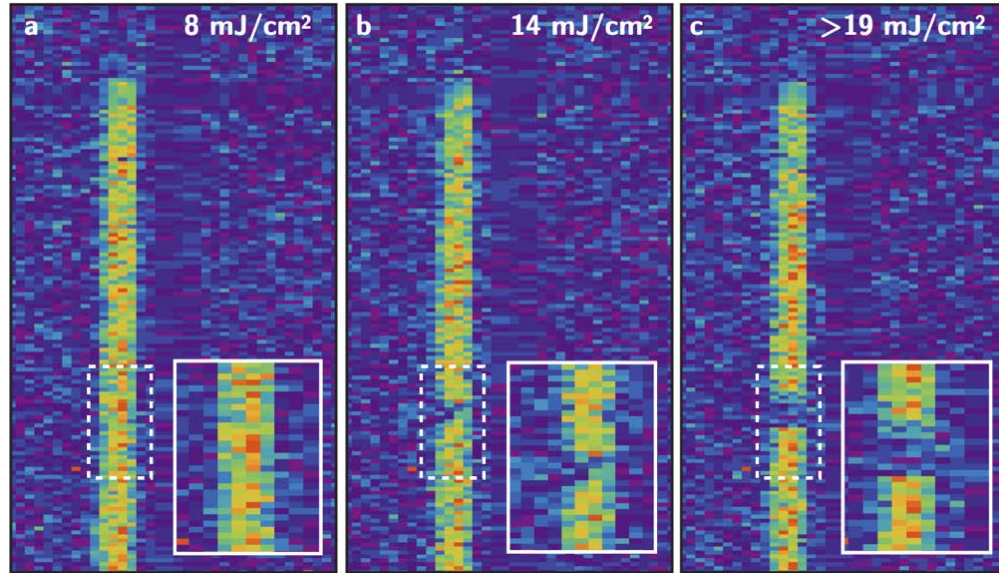

Fig. 3. Recorded (003) peak with different pump fluences (a) 8 mJ/cm^2 (b) 14 mJ/cm^2 (c) > 19 mJ/cm^2. The white dotted rectangle encloses the laser pumped region. The insets show the zoom-in of the pumped region in the diffraction pattern. Note that the 1D X-ray focusing employed in this experiment probes a region larger than the laser-excited area, enabling direct comparison between the pumped and pristine material within the same measurement. The rectangular inset highlights post-mortem changes observed in the (003) diffraction peak of the sample.
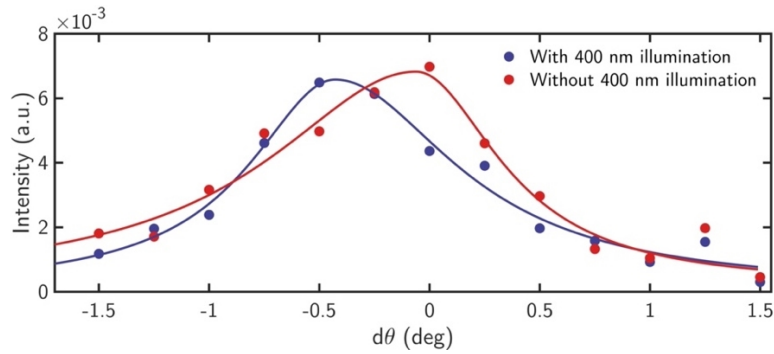
Fig. 4. A permanent shift in the rocking curve of (003) peak induced by the multipulse pump set at fluence slightly higher than F_{th}. θ-scan experiment done with 0.25° step. The dots represent the experimental measurements and the solid line the fitting of the experimental data to a split Lorentzian.

3.1. Threshold fluence for irreversible change

The evaluation of laser-triggered transformation of GaS is essential in view of its potential for photonic applications. We primarily focus on identifying a working regime in which controlled irreversible changes can be imprinted in the material. Pulses from the pump laser illuminates the sample surface for a few tens of seconds (≈ 1000 shots at 100 Hz repetition rate) at fluences < 19 mJ/cm^2, and at normal incidence before the material is probed by X-rays to evaluate its response.

Using the X-ray diffraction setup described in the Methods section, we recorded the diffraction patterns for excitation fluence in the range between 8 and 20 mJ/cm^2. In particular, we monitored the response of the (003) reflection of the $R\bar{3}m$ phase of GaS. The one-dimensional X-ray focusing used in this experiment probed a region that extended beyond the laser-excited area, enabling a direct comparison between the pumped and pristine regions within the same measurement. The results are summarized in Fig. 3, where the rectangular inset highlights post-mortem modifications in the (003) diffraction peak following multi-pulse excitation.

At a fluence up to 8 mJ/cm^2, the X-ray diffraction analysis did not reveal any change to the sample. At a fluence of 14 mJ/cm^2, the X-ray diffraction pattern started to show some local loss of the diffracted X-ray signal in the pumped region. Above 19 mJ/cm^2, the diffraction from the pumped region completely fades away. This experiment thus allows us to determine the laser fluence necessary to permanently change the local structural order of the material, in repetitive pulsed illumination, to about $F_{th} \approx 10$ mJ/cm^2. This fluence threshold defines the upper level of the energy of the laser pump to be deposited in the material for exploring controlled reversible processes.

3.2. Changes in the crystallinity

We further investigate, in more detail, the changes induced in the repetitively pumped sample at fluence closer to the irreversible transformation threshold. Structural changes upon repeated laser surface irradiation of single crystals and materials similar to GaS has been observed previously in various forms [28–30]. It brings complementary information to morphological observations, as done with imaging by optical or electron microscopy of the material following its melting. To analyze such kind of changes in GaS, we thus capture an X-ray diffraction θ-scan rocking curve around the (003) peak (see Fig. 4). The diffraction intensity at each point of the rocking curve was obtained by integrating the diffraction signal and normalizing it with the transmitted beam intensity. The solid line profiles in Fig. 4 represent the fit to a split Lorentzian of the experimental data. The use of asymmetric function in fitting the rocking curves have been

reported on numerous occasions in the past [31,32]. We chose to study this peak because it serves as a potential indicator of lattice distortion along the *c*-axis [001] direction of the material's unit cell.

The shift of the rocking curve towards a smaller diffraction θ-angle value confirms that an irreversible change in the local atomic arrangement has occurred in the GaS sample under this given pump condition. This is unambiguously revealed as all experimental conditions (X-ray and diffracting object) were kept identical between the two diffraction measurements.

The observed shift to smaller θ-angles indicates an increase in the interplanar spacing d_{hkl}. According to Bragg's law, $n\lambda = 2d_{hkl}sin\theta$, a shift of approximately $\Delta\theta \approx 0.5°$ in the rocking curve corresponds to an expanded spacing of $d_{003} \cong 8.46$ Å in the pumped region. This reflects an approximate 10% increase in the original separation between consecutive (003) planes. Consequently, the lattice parameter *c* increases from 23.174 Å to 25.38 Å following multipulse excitation. On the contrary, this shift in the rocking curve is inconsistent with the formation of the energetically close GaS hexagonal phase (2 H phase) for which diffraction pattern also has XRD peaks at the same θ angular region (002 peak). In the case of transformation towards the hexagonal phase, it would have been expected that the peak shifts to higher θ angle, correspondingly to a smaller interplanar distance (see tabulated 2θ values for (002) peak for 2 H phase of GaS in Ref. [5].).

Taken together, these results suggest that repeated illumination with a 400 nm femtosecond laser induces an atomic rearrangement that preserves the in-plane structure but stretches the lattice along the *c*-axis. This elongation is likely driven by thermomechanical stress generated by the laser pulses. The experiment is performed at 100 Hz repetition rate which is longer than the thermal diffusion time occurring typically in microseconds in solids. This suggests that the system gets enough time to relax in between the shots. Therefore, there is negligible impact of the repetition rate on the thermomechanical stress building. Rather than the repetition rates the build-up of stress over the ~1000 accumulations might have contributed to the elongation of the c-axis in GaS. Notably, this type of laser-assisted structural transformation is reported here for the first time in GaS. We propose that the enhanced *c*-axis orientation induced by the 400 nm femtosecond laser, effectively acting as a uniaxial pressure, could be leveraged to strengthen the anisotropic physical properties of GaS, with potential relevance for future applications [33,34].

3.3. Effects on the electronic and optical properties

Building on the discussion in the previous subsection, we carried out *ab-initio* calculations based on density functional theory (DFT) (see Methods for details) to investigate the effect of stretching the *c*-axis of the $R\overline{3}m$ GaS structure, focusing on the changes in its electronic and optical properties. Since experimental XRD data is available for the (003) reflection, we performed structural relaxations by optimizing only the internal atomic coordinates while keeping the lattice parameters fixed. To model the structure in the absence of illumination, we used the lattice parameters reported in Ref. [5]. For the illuminated case, we adopted the *c*-axis experimental value of 25.38 Å. The resulting bond lengths, bond angles, and intra- and interlayer distances schematized in Fig. 1 are summarized in Table 1.

Figure 5 presents the Kohn–Sham independent-particle band structures and total density of states (DOS). Figure 5(a) corresponds to the pristine structure, which exhibits a direct band gap of 1.4 eV at the A point of the Brillouin zone (BZ). In contrast, Fig. 5(b) shows the case with an elongated *c*-axis (with illumination), where the valence band maximum (VBM) shifts along the A-L direction in *k*-space, resulting in an indirect band gap of 1.9 eV, i.e, approximately 0.45 eV larger than that of the pristine structure. Previous studies have extensively explored thickness-dependent bandgap tuning of the 2 H phase of GaS (β-GaS) [3,35] and ε-GaSe [36,37], and highlight the influence of interlayer interactions in the bandgap value. A transition from indirect to direct bandgap with decreasing layers number is well documented for transition metal dichalcogenides

(MoS$_2$, WSe$_2$, WS$_2$, etc.), our calculations point towards a resemblant but swapped feature as a consequence of interlayer distance augmentation. Additionally, a characteristic Mexican-hat dispersion near the VBM, typical of few-layer GaS and other chalcogenides [38,35], is observed here (see inset in Fig. 5(b)) and arises from reduced screening due to the increased interlayer spacing. While it is well known that Kohn–Sham DFT with semi-local exchange–correlation functionals tends to underestimate absolute band gaps, our focus here is on the relative changes, which remain meaningful within this approximation [39].
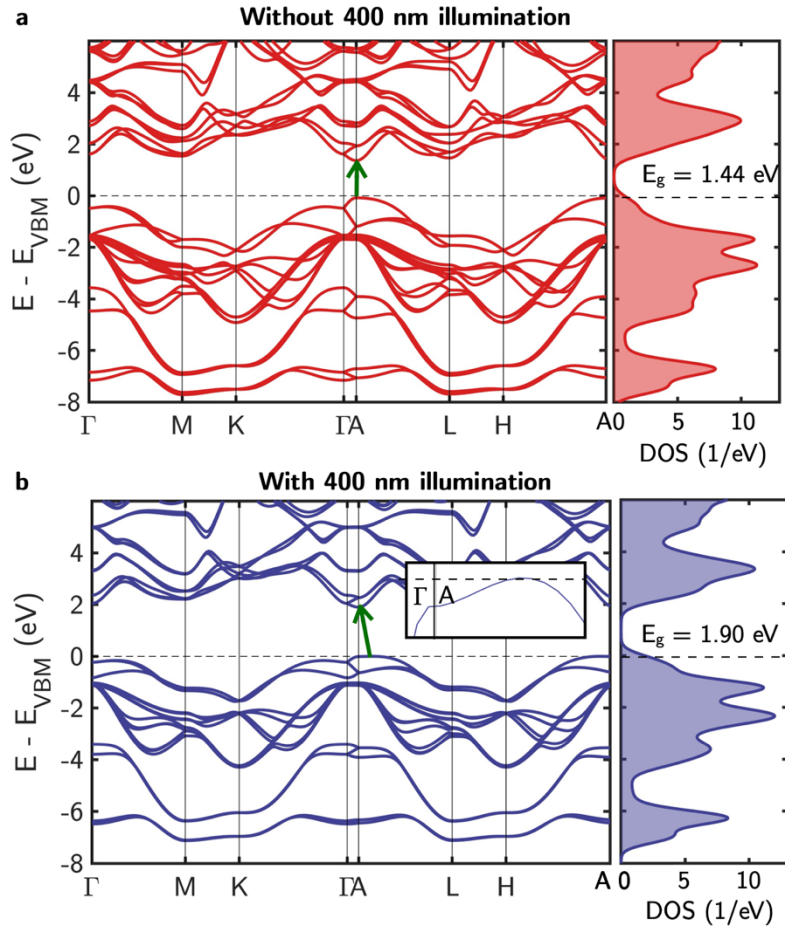

Fig. 5. Electronic dispersion of GaS (a) without and (b) with illumination. The green arrows indicate the lowest energy gap in each case. The inset in (b) shows a Mexican-hat shape of the highest valence band around the valence band maximum.

Figure 6(a) presents the real and imaginary parts of the dielectric function ($\varepsilon = \varepsilon_1 + i\varepsilon_2$) for light polarized parallel to the plane of the $R\bar{3}m$ GaS layers, i.e., the in-plane component. The dielectric function was calculated for both the non-illuminated and illuminated structures. Figure 6(b) shows the corresponding in-plane complex refractive index ($m = n + ik$) over a reduced energy range where optical losses are negligible. While the extinction coefficient k is essentially zero for both cases, the refractive index n differs significantly between the two. To better highlight these differences, Fig. 6(c) displays the refractive index contrast (Δn, Δk) between the studied structures. Such contrasts are crucial for reconfigurable photonics, where local modulation of the refractive index enables tuning of optical responses in photonic devices

[40]. Remarkably, the structural modification yields a nearly constant $\Delta n \approx 0.1$ with $\Delta k = 0$ as a result of the structural modification.
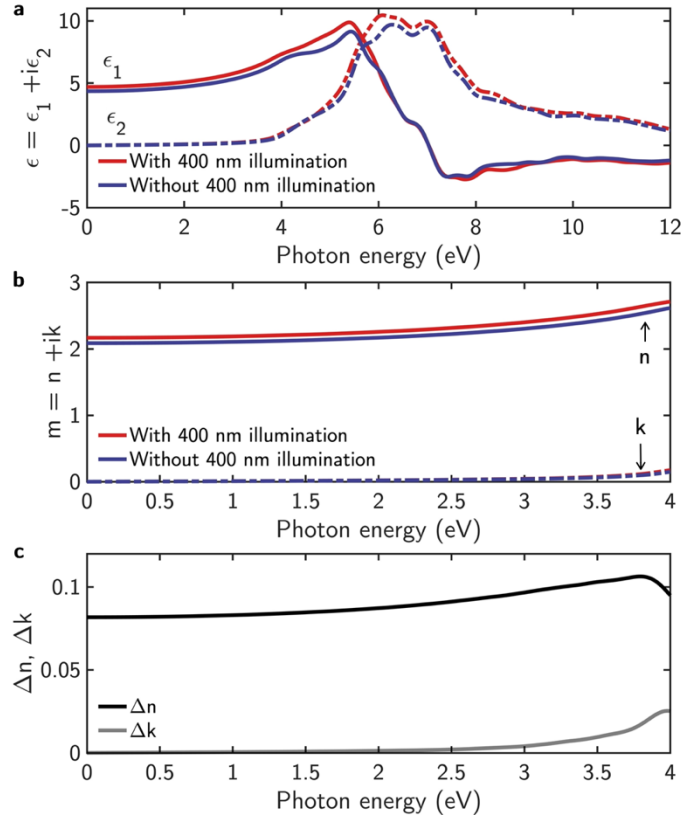

Fig. 6. (a) In-plane real and imaginary parts of the dielectric function ($\epsilon = \epsilon_1 + i\epsilon_2$) of the $R\bar{3}m$ GaS without and with illumination. (b) In-plane real and imaginary parts of the refractive index ($m = n + ik$) of the $R\bar{3}m$ GaS without and with illumination in the low-loss spectral region. (c) Refractive index contrast (Δn, Δk) between the without and with illumination (GaS or cases) in the low-loss spectral region.

It should be noted that this calculation of the optical response, based on a simplified approach using Fermi's Golden Rule (see Methods), neglects local-field effects and excitonic contributions. As such, only the in-plane components are reported, and the results are expected to provide qualitative rather than quantitative agreement [41]. To match the experimental bandgap of 2.55 eV [5], a rigid energy shift of 1.1 eV is applied to both spectra, correcting for the typical underestimation in DFT calculations.

4. Conclusion

We have studied the interaction of a 400-nm femtosecond laser with a $R\bar{3}m$ GaS thin film in repetitive irradiation regime. First, we evaluated the threshold fluence ($F_{th} \approx 10$ mJ/cm^2) from which irreversible changes in GaS structural order occur. At this fluence, rather than getting amorphization of the material, we observed that the initial unit-cell structure is preserved but its interplane spacing along the c-axis elongated. This laser-assisted structural transformation, reported here for the first time in GaS, is likely driven by thermomechanical stress accumulated during multipulse femtosecond laser energy deposition. *Ab initio* calculations reveal that this

elongation leads to a transition from a direct to an indirect band gap, with an increase of approximately 0.45 eV. Optical calculations show that this structural change induces a nearly constant in-plane refractive index contrast of $\Delta n \approx 0.1$ over the spectral region with negligible losses, a promising feature for reconfigurable photonic applications. We believe this work lays the groundwork for future investigations into light-induced structural dynamics in GaS at the atomic level and for the development of laser-assisted patterning techniques in 2D chalcogenides.

Data availability. The data underlying this study are openly available at [42].

References

1. A. Singh, S. S. Jo, Y. Li, *et al.*, "Refractive uses of layered and two-dimensional materials for integrated photonics," ACS Photonics **7**(12), 3270–3285 (2020).
2. Y. Gutiérrez, S. Dicorato, E. Dilonardo, *et al.*, "Stability of nanometer-thick layered gallium chalcogenides and improvements via hydrogen passivation," ACS Appl. Nano Mater. **6**(21), 20161–20172 (2023).
3. Y. Gutiérrez, D. Juan, S. Dicorato, *et al.*, "Layered gallium sulfide optical properties from monolayer to CVD crystalline thin films," Opt. Express **30**(15), 27609–27622 (2022).
4. Y. Gutiérrez, M. M. Giangregorio, S. Dicorato, *et al.*, "Exploring the thickness-dependence of the properties of layered gallium sulfide," Front. Chem. **9**, 781467 (2021).
5. Y. Gutiérrez, F. Agresti, D. Juan, *et al.*, "Unveiling Polymorphs and Polytypes of the 2D Layered Semiconducting Gallium Monosulfide," Adv. Opt. Mater. **12**(15), 2303002 (2024).
6. S. Yang, Y. Li, X. Wang, *et al.*, "High performance few-layer GaS photodetector and its unique photo-response in different gas environments," Nanoscale **6**(5), 2582–2587 (2014).
7. P. Hu, L. Wang, M. Yoon, *et al.*, "Highly responsive ultrathin GaS nanosheet photodetectors on rigid and flexible substrates," Nano Lett. **13**(4), 1649–1654 (2013).
8. T. Chen, Y. Lu, Y. Sheng, *et al.*, "Ultrathin all-2D lateral graphene/GaS/graphene UV photodetectors by direct CVD growth," ACS Appl. Mater. Interfaces **11**(51), 48172–48178 (2019).
9. Y. Lu, J. Chen, T. Chen, *et al.*, "Controlling defects in continuous 2D GaS films for high-performance wavelength-tunable UV-discriminating photodetectors," Adv. Mater. **32**(7), 1906958 (2020).
10. S. Dicorato, Y. Gutiérrez, M. M. Giangregorio, *et al.*, "Interplay between thickness, defects, optical properties, and photoconductivity at the centimeter scale in layered GaS," Nanomaterials **12**(3), 465 (2022).
11. S. Ahmed, P. K. Cheng, J. Qiao, *et al.*, "Nonlinear optical activities in two-dimensional gallium sulfide: a comprehensive study," ACS Nano **16**(8), 12390–12402 (2022).
12. M. I. Zappia, G. Bianca, S. Bellani, *et al.*, "Two-dimensional gallium sulfide nanoflakes for UV-selective photoelectrochemical-type photodetectors," J. Phys. Chem. C **125**(22), 11857–11866 (2021).
13. A. Harvey, C. Backes, Z. Gholamvand, *et al.*, "Preparation of gallium sulfide nanosheets by liquid exfoliation and their application as hydrogen evolution catalysts," Chem. Mater. **27**(9), 3483–3493 (2015).
14. K. Guo, Q. Yu, F. Liu, *et al.*, "Synthesis of hexagonal structured GaS nanosheets for robust femtosecond pulse generation," Nanomaterials **12**(3), 378 (2022).
15. Y. Gutiérrez, S. Dicorato, A. P. Ovvyan, *et al.*, "Layered Gallium Monosulfide as Phase-Change Material for Reconfigurable Nanophotonic Components On-Chip," Adv. Opt. Mater. **12**(3), 2301564 (2024).
16. H. Lu, Y. Chen, K. Yang, *et al.*, "Ultrafast nonlinear optical response and carrier dynamics in layered gallium sulfide (GaS) single-crystalline thin films," Front. Mater. **8**, 775048 (2021).
17. O. Utéza, P. Blandin, L. Charmasson, *et al.*, "ASUR: Plateforme d'Applications des Sources laser Ultra-Rapides pour l'imagerie X et l'interaction laser-matière." In UVX 2012-11e Colloque sur les Sources Cohérentes et Incohérentes UV, VUV et X; Applications et Développements Récents, p. 01004. EDP Sciences, 2013.
18. D. R. Hamann, M. Schlüter, and C. Chiang, "Norm-conserving pseudopotentials," Phys. Rev. Lett. **43**(20), 1494–1497 (1979).
19. P. Giannozzi, S. Baroni, N. Bonini, *et al.*, "QUANTUM ESPRESSO: a modular and open-source software project for quantum simulations of materials," J. Phys.: Condens. Matter **21**(39), 395502 (2009).
20. V. R. Cooper, "Van der Waals density functional: An appropriate exchange functional," Phys. Rev. B **81**(16), 161104 (2010).
21. K. Lee, É. D. Murray, L. Kong, *et al.*, "Higher-accuracy van der Waals density functional," Phys. Rev. B **82**(8), 081101 (2010).
22. D. R. Hamann, "Optimized norm-conserving Vanderbilt pseudopotentials," Phys. Rev. B **88**(8), 085117 (2013).

23. L. Kleinman and D. M. Bylander, "Efficacious form for model pseudopotentials," Phys. Rev. Lett. **48**(20), 1425–1428 (1982).

24. M. J. Van Setten, V. A. Popa, G. A. De Wijs, *et al.*, "Electronic structure and optical properties of lightweight metal hydrides," Phys. Rev. B **75**(3), 035204 (2007).

25. H. J. Monkhorst and J. D. Pack, "Special points for Brillouin-zone integrations," Phys. Rev. B **13**(12), 5188–5192 (1976).

26. M. P. Pardo and J. Flahaut, "A New Variety of Gas, Rhombohedral 3R Metastable-Formation and Structural Study," Mater. Res. Bull. **22**(3), 323–329 (1987).

27. Y. Liu, Y. Liu, and M. G. Drew, "Comparison of calculations for interplanar distances in a crystal lattice," Crystallography Rev. **23**(4), 252–301 (2017).

28. X. Sedao, M. V. Shugaev, C. Wu, *et al.*, "Growth twinning and generation of high-frequency surface nanostructures in ultrafast laser-induced transient melting and resolidification," ACS Nano **10**(7), 6995–7007 (2016).

29. J. Vincenc Oboňa, V. Ocelik, J. C. Rao, *et al.*, "Modification of Cu surface with picosecond laser pulses," Appl. Surf. Sci. **303**, 118–124 (2014).

30. O. Salicio, C. Wiemer, M. Fanciulli, *et al.*, "Effect of pulsed laser irradiation on the structure of GeTe films deposited by metal organic chemical vapor deposition: A Raman spectroscopy study," J. Appl. Phys. **105**(3), 033520 (2009).

31. S. A. Howard and R. L. Snyder, "An evaluation of some profile models and the optimization procedures used in profile fitting," Adv. X-ray Anal. **26**, 73–80 (1982).

32. R. W. Cheary, A. A. Coelho, and J. P. Cline, "Fundamental parameters line profile fitting in laboratory diffractometers," J. Res. Natl. Inst. Stand. Technol. **109**(1), 1 (2004).

33. P. Khan and K. V. Adarsh, "Light-induced effects in amorphous chalcogenide glasses: Femtoseconds to seconds," Physics **3**(2), 255–274 (2021).

34. S. V. Zabotnov, P. K. Kashkarov, A. V. Kolobov, *et al.*, "Structural transformations and formation of microstructures and nanostructures in thin films of chalcogenide vitreous semiconductors," Nanobiotechnol. Rep. **18**(6), 829–841 (2023).

35. D. Wickramaratne, F. Zahid, and R. K. Lake, "Electronic and thermoelectric properties of van der Waals materials with ring-shaped valence bands," J. Appl. Phys. **118**(7), 075101 (2015).

36. D. V. Rybkovskiy, N. R. Arutyunyan, A. S. Orekhov, *et al.*, "Size-induced effects in gallium selenide electronic structure: The influence of interlayer interactions," Phys. Rev. B **84**(8), 085314 (2011).

37. Y. Ma, Y. Dai, M. Guo, *et al.*, "Tunable electronic and dielectric behavior of GaS and GaSe monolayers," Phys. Chem. Chem. Phys. **15**(19), 7098–7105 (2013).

38. M.-W. Chen, H. Kim, D. Ovchinnikov, *et al.*, "Large-grain MBE-grown GaSe on GaAs with a Mexican hat-like valence band dispersion," npj 2D Mater. Appl. **2**(1), 2 (2018).

39. W. An, F. Wu, H. Jiang, *et al.*, "Systematic investigation on topological properties of layered GaS and GaSe under strain," The J. Chemical Phys. **141**(8), 084701 (2014).

40. M. Wuttig, H. Bhaskaran, and T. Taubner, "Phase-change materials for non-volatile photonic applications," Nat. Photonics **11**(8), 465–476 (2017).

41. D. Juan, Y. Gutiérrez, P. G. Fernández, *et al.*, "Excitonic Features in the Optical Response of Layered Gallium Sulphide," In *2023 International Semiconductor Conference (CAS)*, pp. 125–128. IEEE, 2023.

42. K. P. Khakurel, R. Clady, S. Espinoza, *et al.*, "Engineering GaS crystal anisotropy via ultrafast laser excitation: data," Zenodo, 2023, 10.5281/zenodo.15704088.